Nonaxisymmetric field effects on Alcator C-Mod[a)]

S. M. Wolfe,[b)] I. H. Hutchinson, R. S. Granetz, J. Rice, and A. Hubbard
Plasma Science and Fusion Center, Massachusetts Institute of Technology, Cambridge, Massachusetts 02139

A. Lynn and P. Phillips
Fusion Research Center, University of Texas at Austin, Austin, Texas 78712

T. C. Hender and D. F. Howell
UKAEA Fusion Association, Culham Science Centre, Abingdon, Oxon OX14 3DB, United Kingdom

R. J. La Haye and J. T. Scoville
General Atomics, San Diego, California 92186

(Received 19 November 2004; accepted 1 February 2005; published online 13 April 2005)

A set of external coils (A-coils) capable of producing nonaxisymmetric, predominantly $n=1$, fields with different toroidal phase and a range of poloidal mode m spectra has been used to determine the threshold amplitude for mode locking over a range of plasma parameters in Alcator C-Mod [I. H. Hutchinson, R. Boivin, F. Bombarda, P. Bonoli, S. Fairfax, C. Fiore, J. Goetz, S. Golovato, R. Granetz, M. Greenwald *et al.*, Phys. Plasmas **1**, 1511 (1994)]. The threshold perturbations and parametric scalings, expressed in terms of (B_{21}/B_T), are similar to those observed on larger, lower field devices. The threshold is roughly linear in density, with typical magnitudes of order 10^{-4}. This result implies that locked modes should not be significantly more problematic for the International Thermonuclear Experimental Reactor [I. P. B. Editors, Nucl. Fusion **39**, 2286 (1999)] than for existing devices. Coordinated nondimensional identity experiments on the Joint European Torus [Fusion Technol. **11**, 13 (1987)], DIII-D [Fusion Technol. **8**, 441 (1985)], and C-Mod, with matching applied mode spectra, have been carried out to determine more definitively the field and size scalings. Locked modes on C-Mod are observed to result in braking of core toroidal rotation, modification of sawtooth activity, and significant reduction in energy and particle confinement, frequently leading to disruptions. Intrinsic error fields inferred from the threshold studies are found to be consistent in amplitude and phase with a comprehensive model of the sources of field errors based on "as-built" coil and bus-work details and coil imperfections inferred from measurements using *in situ* magnetic diagnostics on dedicated test pulses. Use of the A-coils to largely cancel the 2/1 component of the intrinsic nonaxisymmetric field has led to expansion of the accessible operating space in C-Mod, including operation up to 2 MA plasma current at 8 T. © *2005 American Institute of Physics*. [DOI: 10.1063/1.1883665]

I. INTRODUCTION

Small deviations from axisymmetry in the magnetic field of tokamak devices are well known to destabilize nonrotating tearing modes (locked modes) which can significantly impact plasma operation. Error-field induced locked modes can be responsible for disruptions as well as degradation of confinement. In present experiments these modes are found to restrict the available operating space, particularly in ohmically heated discharges at low density. The impact of these modes on the operation of future burning plasma experiments, such as the International Thermonuclear Experimental Reactor (ITER),[1] has been a matter of concern; key issues are prediction of the error-field sensitivity of such devices, and determination of the requirements for corrective measures.

In this paper, we report on recent experiments at Alcator C-Mod[2] which extend locked mode studies to the range of toroidal field of proposed burning plasma devices. The results, taken along with studies on other tokamaks, provide improved constraints on predictions for locked more thresholds on ITER. Experiments employing externally generated compensation fields have successfully increased the range of accessible parameters in C-Mod.

A. Background: Experiment

Experimental investigations of plasma response to static nonaxisymetric perturbations have been carried out on a number of tokamaks.[3–9] The externally induced locked modes observed in these experiments are found to be predominately $m=2$, $n=1$. Typical threshold perturbations are found to be $B_{21}/B_T \sim 10^{-4}$, and the experiments indicate that the threshold scales approximately linearly with plasma density. Scaling with toroidal field, device size, and safety factor q have also been investigated, with less uniformly consistent results,[1,4] making extrapolation to future devices somewhat problematic.

[a)]Paper BI1 4, Bull. Am. Phys. Soc. **49**, 20 (2004).
[b)]Invited speaker. Electronic mail: wolfe@psfc.mit.edu

B. Background: Theoretical

The theoretical description[3,10–16] of error-field induced locked modes is rather well developed, and only a sketch of the main aspects of the problem is presented here. In the absence of rotation, the response of a tearing-stable plasma to a static nonaxisymmetric field perturbation results in the formation (on the resistive time scale) of a static island whose size will typically be greater than that of the "vacuum island" calculated by naively superposing the vacuum perturbation on the equilibrium field.[3] In a rotating plasma, helical currents are induced in the rational surface $q_s=m/n$ which oppose the perturbation and inhibit island formation. Finite resistivity introduces a phase shift that gives rise to a $\tilde{j}\times\tilde{B}$ torque, which in steady-state must be balanced by viscous drag (and any externally applied torque). For small perturbing fields, the rotation frequency remains close to its "natural" value ω_0 (*evaluated in the lab frame*). When the external perturbation is sufficiently large to slow the rotation to about $\omega_0/2$, the island grows nonlinearly and the plasma rotation slows abruptly to lock to the frame of the perturbation. This effect is generally called "mode penetration." The relative magnitude of the critical helically resonant field obtained from torque balance can be parametrized as

$$\frac{B_{\perp mn}}{B_T} \propto \omega_0 \tau_A \left(\frac{\tau_{rec}}{\tau_v}\right)^{1/2}, \tag{1}$$

where $\tau_A=R\sqrt{\mu_0 n_i(r_s)m_i}/B$ is the Alfvén time evaluated at the rational surface, τ_{rec} the reconnection time, which depends on resistivity and viscosity,[13] and $\tau_v=r_s^2/\nu_\perp$ the viscous diffusion time.

Some aspects of the dependence of the mode penetration threshold on plasma parameters are apparent from the form of Eq. (1). For a given perturbation, locking is favored at lower density, as the electromagnetic torque is applied in slowing less mass. Driven rotation, as by neutral beams, increases ω_0 and therefore the magnitude of the required perturbation; in the absence of bulk rotation the natural rotation frequency for a tearing mode[17] is expected to be of the order $\omega_0\approx\omega_{De}\propto T_e/a^2B_T$, so the sensitivity to error fields might be expected to be greater as device size and field increase. The dependence of the locking threshold on size and field may be estimated[3,5,18] by assuming a confinement scaling and making further assumptions regarding the scaling of viscosity and rotation effects.

In general, error fields in tokamaks exhibit a broad poloidal mode spectrum, and the interaction of multiple m values must be considered. In a toroidal system, mode coupling leads to an effective field at the $q=m/n$ surface due to components at $m\pm1$. Additionally, electromagnetic drag at adjacent flux surfaces, e.g., $q=1$, 3 can couple to the $q=2$ surface through plasma viscosity, reducing the amount of direct drag required for penetration. The expression (1) should therefore theoretically be modified by replacing the single mode field $B^2_{\perp mn}$ by an effective field for mode penetration

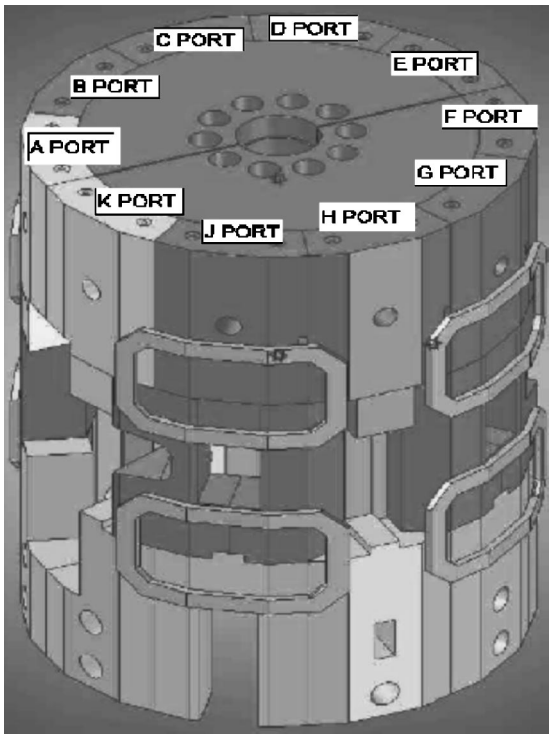

FIG. 1. Nonaxisymmetric field coils (A-coils) are mounted to the concrete igloo surrounding the tokamak. Pairs of coils are located above and below the midplane at four toroidal locations.

$$B^2_{\text{pen}} = \left|\sum_m B_m C_m\right|^2 + \sum_{k\neq 2} |B_k|^2 V_k, \tag{2}$$

where the first term represents the contribution to the direct electromagnetic torque at the $q=2$ surface, the second the viscous torque, the C_m are (in general complex) coupling coefficients and the V_k real positive viscous coupling terms, and we have assumed $n=1$ and the subscript n has been dropped for clarity. Experiments on DIII-D[6,7,18] and Compass-D[4] were analyzed by fitting the coefficients for the terms in B_{11} and B_{31}, demonstrating the significance of these "sideband" terms.

II. C-MOD NONAXISYMMETRIC COILSET

The high field ($B_T\leqslant 8.1$ T) and compact size ($R_0\approx 0.67$ m, $a\approx 0.21$ m) of Alcator C-Mod[2] enable exploration of locked mode effects, breaking the covariance between field and size of prior studies. The typical C-Mod operating field of 5.3 T is the same as ITER, while the ratio of spatial scales is about 1/9.

A set of coils[19] capable of producing nonaxisymmetric (predominately $n=1$) fields with a variety of toroidal phases and a range of poloidal mode spectra was installed on Alcator C-Mod in 2003. This coilset (the "A-coils") was installed in response to observations of locked modes during experiments at low density ($\overline{n_e}\leqslant 5\times10^{19}$ m^{-3}) and/or high current ($I_p>1.2$ MA), and was designed to serve as a corrective tool as well as providing new capabilities for investigating the physics of locked modes.

The A-coils, shown schematically in Fig. 1, are wound from AWG No. 0000 welding cable[20] enclosed in aluminum

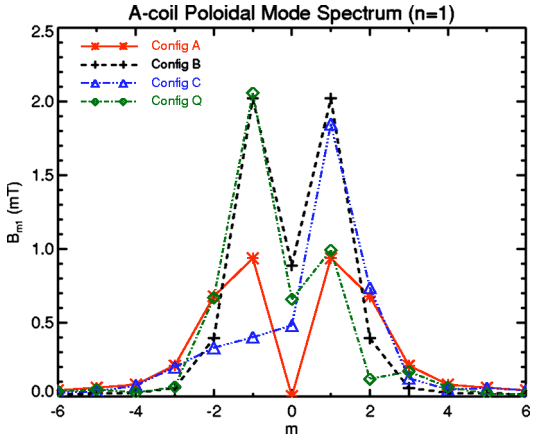

FIG. 2. (Color online). Calculated mode amplitudes for $n=1$ with different combinations of four A-coils in series with current of 2.3 kA. Positive m corresponds to the resonant helicity.

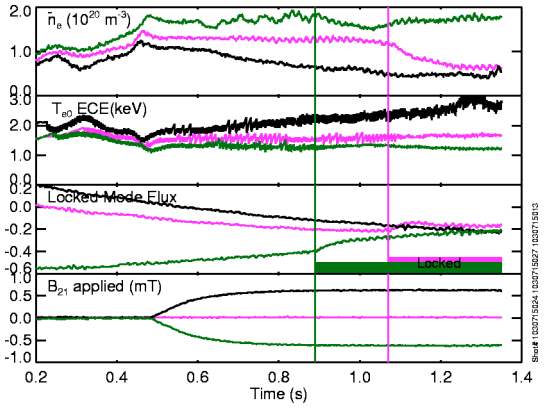

FIG. 3. (Color online). Time histories of locked mode suppression and excitation. The traces labeled "locked mode flux" are difference signals of a pair of toroidally antisymmetric saddle loops measuring radial field at the outboard midplane. Signatures of mode locking (color/shaded traces) include decreasing density and modification of the central sawtooth behavior, as well as the response seen on the magnetic diagnostics. The black traces show no locked mode down to $\overline{n_e}\sim 4\times 10^{19}$ m^{-3}, indicating good compensation of the intrinsic error.

coilcases and mounted on the outside of the concrete radiation shield (igloo) which surrounds the tokamak. The full coilset consists of eight coils consisting of 27 turns each in a racetrack shape. (Only seven coils were installed for the experiments reported here, reducing the experimental flexibility but not otherwise impacting the results.) The coils can be connected in a variety of configurations, allowing a range of phase and helicity as well as different poloidal mode spectra. The maximum current available from the single power supply used for these experiments was 3700 A per turn.

Examples of accessible mode structures, evaluated at the $q=2$ surface for a typical C-Mod equilibrium, are shown in Fig. 2 for several coil combinations. Here the helical Fourier components in straight field line geometry are defined as

$$B_{mn}=\frac{1}{2\pi^2}\int_0^{2\pi}d\phi\int_0^{2\pi}d\hat{\theta}\,B_\perp(\phi,\hat{\theta})e^{-j(n\phi+m\hat{\theta})}, \tag{3}$$

where $B_\perp$ is the field normal to the rational surface and the poloidal angle is given by $\hat{\theta}=(1/q)\oint dl(B_\phi/RB_p)$, with $\hat{\theta}=0$ corresponding to the outboard midplane. The field produced by the A-coil is dominantly in the low m numbers, $|m|=1$, 2, with a smaller contribution at $m=3$; the ratio of $m=1$ to $m=2$ can be varied over a factor of 5 by suitable choice of coil connections.

The location of the A-coils was chosen for reasons of accessibility, to allow the coils to be installed without disassembling the tokamak during a relatively brief hiatus in operation. The large separation between the coils and the plasma $(R_{coil}\approx 2.5\text{ m}, R_{plasma}\approx 0.67\text{ m})$ accounts for the rapid falloff of higher-order poloidal modes $m\geqslant 3$ in the spectrum. An additional consequence of the chosen location is that the coils are outside of the stainless steel cylinder and domes which provide the structural support for the toroidal field magnet, resulting in a substantial field "soak-through" time due to eddy currents in the superstructure; measurements of the response to the A-coils of magnetic diagnostics inside the C-Mod vacuum vessel indicate a lag of between 70 and 110 ms, which must be incorporated in analysis of transient data.

III. INTRINSIC ERROR FIELDS

A. Locked mode excitation/suppression experiments

Experiments using the A-coils in different configurations to suppress and excite locked modes were carried out in order to assess the efficacy of the coils and provide an estimate of the locking threshold and the intrinsic error. The first experiments were carried out at a field of 5.4 T and plasma current of 1 MA, and indicated that application of the mode spectrum shown as Config. *A* in Fig. 2 was effective at suppressing a naturally occurring locked mode. The orientation of the 2/1 component of this coil configuration, i.e., the phase of the complex Fourier component, is $\approx 23°$, which implies that the intrinsic error is oriented to the third quadrant, toward E-port (see Fig. 1). Application of reverse current in the same coil configuration resulted in excitation of a locked mode in a passively stable plasma at higher density, as shown in Fig. 3.

Subsequent experiments, employing a total of eleven different coil configurations to vary the orientation of the applied field, were carried out to better define the magnitude and orientation of the intrinsic nonaxisymmetric field and to ascertain the locking threshold in terms of the total 2/1 component. These experiments were conducted at a toroidal field and current of 4.1 T and 600 kA, with line-averaged densities $3.2<\overline{n_e}<5.4\times 10^{20}$ m^{-3}. The results are shown in Fig. 4. These data are consistent with a locking threshold of about 3.5×10^{-4} T, and an intrinsic error field again oriented in the third quadrant at an angle of $\approx -135°$. The parameters of this experiment were chosen to make the origin (zero applied field) a threshold point. The radius of the unlocked circle increases with density.

B. Source model

These experiments indicated the presence of an intrinsic error field with a 2/1 amplitude of a few 10^{-4} T, oriented in the third quadrant. The experiments also suggested that the

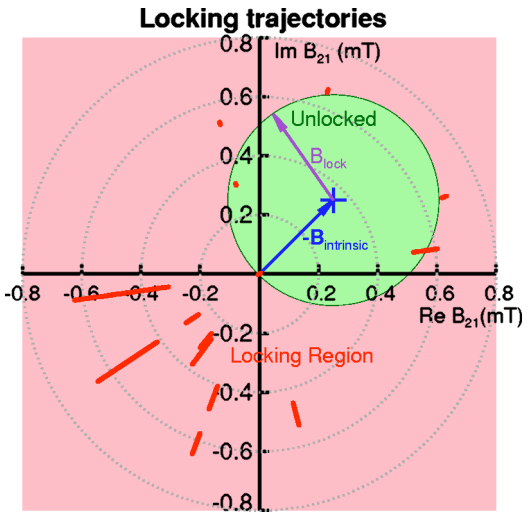

FIG. 4. (Color online). Applied 2/1 field magnitude and orientation resulting in mode locking for discharges at $B=4.1$ T, $I_p=600$ kA, $\bar{n}_e \approx 4\times10^{19}$ m^{-3}. The solid circle enclosing the unlocked (stable) region has radius $B_{21}^{\mathrm{lock}} \approx 3.5\times10^{-4}$ T and origin $-B_{21}^{\mathrm{intrin}} \approx 2.5\times10^{-4}$ T $\exp(j\pi/4)$.

error fields evolve on the time scale of a plasma pulse. A number of possible sources for this error field have been considered.

Review of the tokamak design and fabrication records indicate the existence of several nonaxisymmetric current paths. Significant contributions ($B_{21}\sim 2\times10^{-4}$ T) were calculated for the toroidal field bus and the layer-to-layer transitions in the central OH solenoid. The bus work feeding the OH solenoid was also found to contribute a helical component amounting to about 10% of the effect due to the winding asymmetries. In addition, smaller effects were found based on the design of the current feeds for the poloidal field (EF) ring coils; calculations indicated that these would contribute measurable local fields at the magnetic diagnostics, but have a negligible ($B_{21}<10^{-5}$ T) in the plasma region. The orientation of the calculated $m=2$, $n=1$ components due to these known asymmetries is consistent with the inferred error fields based on the detailed locking and compensation studies described in Sec. III A, but the magnitudes are smaller by a factor of 2–3.

A potential additional, undocumented, source of nonaxisymmetric error fields arises from unavoidable positioning or manufacturing errors in the poloidal field coil system. The Alcator C-Mod poloidal field (PF) set consists of the three-component central (OH) solenoid, the equilibrium field (EF-1, 2, 3, and EF-C) ring coil pairs, which are located inside the toroidal field (TF) magnet and mounted on the vacuum vessel, and an additional pair of ring coils (EF-4) mounted outside the TF on the structural cylinder. The design positioning tolerance for these coils is of the order of millimeters, but no as-built survey of the actual locations at this scale of accuracy is available. We have therefore attempted to estimate the deviations of these coils based on *in situ* magnetic measurements.

Nonaxisymmetric positioning errors of each of the principal components of the PF system is modeled as a combination of rigid $n=1$ tilts and shifts, as in La Haye and Scoville.[21] Because in C-Mod the location of the coils is potentially affected by the cryogenic environment, we have chosen to measure the nonaxisymmetric field under normal run conditions, using our standard equilibrium diagnostic sensors mounted on the walls of the vacuum vessel. These loops are located at 26 poloidal locations in each of four toroidal arrays at angles $\phi=54°$, 126°, 234°, 306°. Individual PF coils were energized on successive shots, with the tokamak under vacuum and at normal operating temperature; pulse lengths of 1–2 s were used to allow evaluation of field penetration effects. Of the nominal 104 poloidal field (B_p) sensors, a total of 77 loops (51 pairs) were operational for this experiment. The basic measurements for the analysis consist of the *difference signals* of pairs of B_p loops at the same poloidal locations, corrected for "known" design asymmetries, as discussed above. The observed difference signals are of the order of 10^{-3} of the absolute signal levels, while the loop calibration is nominally ±0.5%, and the calibration of the integrators also has a nominal uncertainty of ±0.5%. Furthermore, discrepancies in placement or orientation of the sensor loops would mimic PF coil position errors. *Differential* gains, displacements, and tilts of the sensor pairs are therefore also fitted as part of the model.

Once these additional fitting parameters are included, the analysis for the PF coil displacements consists of a 663×248 weighted linear least-square regression problem, where the data contain 51 difference signals Δ_{ij} for each of 13 pulses, and the model comprises: four tilt and shift parameters (sin and cos parameters) for each of 11 PF coils, 51 gain/calibration discrepancies δG_{ij}, and 3×51 relative displacement and tilt discrepancies $(\delta R_{ij}, \delta Z_{ij}, \delta\theta_{ij})$. This system was solved by truncated singular value decomposition (TSVD),[22] with 240 of 248 principal vectors being retained. The resulting χ^2 is 347 with 423 degrees of freedom. The results are plausible with respect to assembly tolerances, with maximum displacements of the order of a few millimeters. For typical discharges, these tilts and shifts correspond to $n=1$ field perturbations of a few times 10^{-4} T. Magnitudes and orientation of the individual contributions to $m=1$, 2, 3 for a typical 1 MA discharge are shown in Fig. 5. The largest contributions come from the OH1, the principal component of the central solenoid, for which the current increases during the pulse to provide the inductive flux swing; and the EF2L, and EF3L coils which provide shaping and equilibrium field, and whose current is nearly constant during the flattop of the plasma current.

The combined calculated contributions from the "as-built" nonaxisymmetric currents and the PF coil displacements inferred from magnetic measurements of single coil test shots seem consistent, within errors, in magnitude and orientation, with the results of locked mode experiments using the A-coils described in Sec. III A. Some systematic residual discrepancies may be explained by variation of the model terms within their uncertainties, or by inclusion of additional source terms not included in the above analysis.

Among the potential sources not addressed by the previous analysis is the possibility of asymmetries associated with the TF magnet itself. We have no capability of measuring such effects with presently installed diagnostics; nonaxisym-

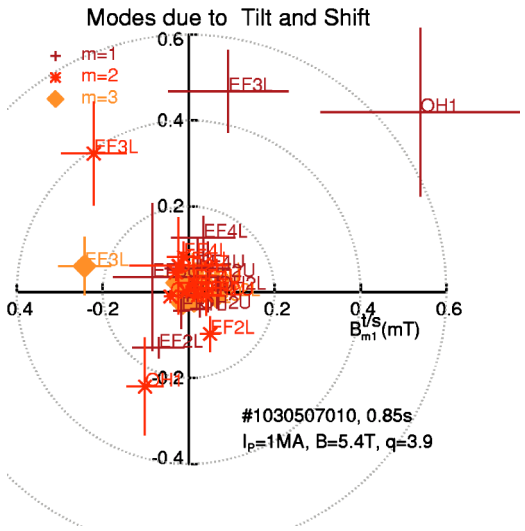

FIG. 5. (Color online). Mode amplitudes and orientation due to tilts and shifts of the poloidal field coils for a typical discharge.

metric responses are seen on the magnetic loops during toroidal field pulses, but there is no way to distinguish a true nonaxisymmetric field effect from differential tilts of the B_p loops in the toroidal direction. Another potential effect is the fact that the modeling we have carried out of necessity excluded the possibility of $n \geqslant 2$ fields associated with the PF coils. These might arise, for example, due to out-of-round or bowing deformations of the ring coils; if present, these would be aliased into the pure $n=1$ calculation and produce erroneous results for the shift and tilt parameters.

Another possible cause of discrepancies between calculations of intrinsic error from the source model and inferences from locking threshold studies is that the latter have been analyzed in terms of the effect of the (2,1) mode only. As noted in Sec. I B, sideband effects are expected to play a role, and since the $m=1$ and $m=3$ components of the intrinsic error field will not in general have the same relative amplitude or orientation as those of the A-coils, the inferred intrinsic error based on consideration of the applied (2,1) field alone may be misleading. Indeed, as seen in Fig. 6,

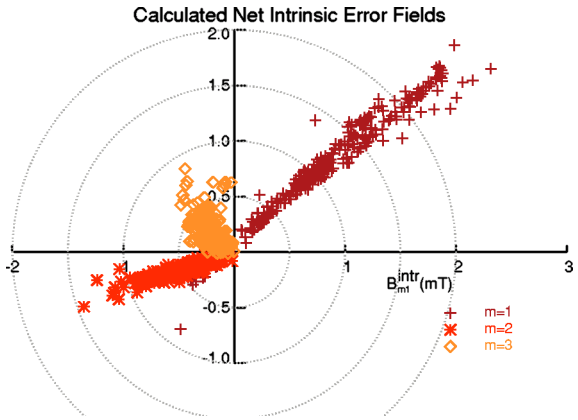

FIG. 6. (Color online). Orientation and magnitude of the first three poloidal modes of the calculated $n=1$ intrinsic error fields for the entire C-Mod locked mode database.

while the calculated (2,1) component of the intrinsic error field lies in the third quadrant, consistent with the experimental results of Sec. III A, the $m=3$, $n=1$ term is in quadrant 2, approximately perpendicular to the (2,1), while the (1,1) is in quadrant 1, about 160° from the (2,1) component. The A-coil sideband components, on the other hand, are aligned with the (2,1), Thus, an applied field that compensates the intrinsic (2,1) component must largely augment the (1,1) term.

IV. EXPERIMENTAL RESULTS

A. Locking and mode penetration

Mode locking behavior observed on C-Mod is similar in most respects to observations on lower field devices. Onset of the mode is often, though not always, observed as nonaxisymmetric perturbations on external magnetics signals, including saddle coils sensitive to radial flux at the outboard midplane and B_p loops oriented parallel to the vessel wall. In addition, the core rotation, monitored by x-ray Doppler measurements of hydrogen-like and helium-like argon ions, slows to zero. The density typically falls, as does the global stored energy, as both particle and energy confinement is reduced.

A nearly ubiquitous signature of mode locking on Alcator C-Mod is a modification of the sawtooth behavior. In some cases the sawteeth are completely suppressed, but in others the sawtooth amplitude and period are reduced, while the inversion radius is essentially unchanged.

An example of the effect of the locked island on the electron temperature profile is shown in Fig. 7. The flattened region appears to be located just inside the $q=2$ surface based on the EFIT equilibrium reconstruction. The width of the flattened region, which in this case is about 2 cm, places only a lower bound on the actual island width, since the electron cyclotron emission view is probably not looking at the O-point. The growth time of the island, as evidenced by both the profile change, and the antisymmetric magnetic signal, is about 100 ms.

B. Scaling of locked mode threshold

The C-Mod locked mode database presently contains over 300 timeslices, covering a substantial range of plasma parameters: $0.27 \leqslant \overline{n_e} \leqslant 6.2 \times 10^{20}$ m^{-3}, $2.5 \leqslant B_T \leqslant 8.1$ T, $2.4 \leqslant q_{95} \leqslant 10$, $0.3 \leqslant I_p \leqslant 2$ MA. Experiments have been carried out using the A-coils to provide $0 \leqslant |B_{21}/B_T| \leqslant 3.6 \times 10^{-4}$. The dataset consists mainly of lower single null, ohmic discharges, with a smaller number of upper null cases and a few plasmas with ICRF (ion cyclotron range of frequency) heating. Most discharges are L mode, although a few H modes, ohmic and rf-heated, are included. In all the cases considered here, the q profile is monotonic with $q_0 \leqslant 1$, and sawteeth are present before locking.

The locked mode database contains approximately equal numbers of locked and unlocked cases. These data include locked modes observed both with and without the use of the A-coils. Typically, experiments employing the A-coil are conducted by applying a constant nonaxisymmetric perturba-

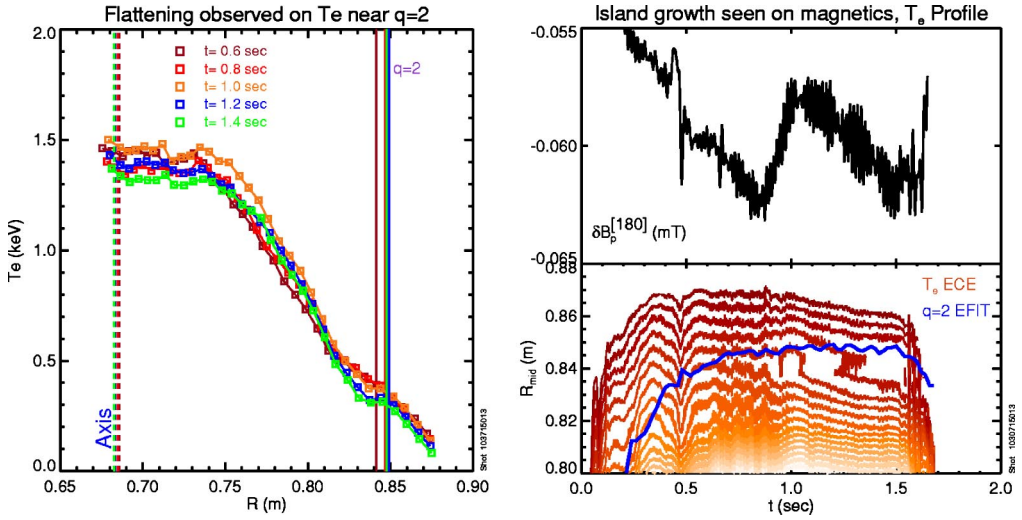

FIG. 7. (Color online). Electron temperature profiles showing flattening just inside the nominal $q=2$ radius. The radiometer view is from below the midplane at toroidal angle $\phi=180°$. The magnetic signal is the difference of two BP loops on the inner wall at $\phi=54$, 234°.

tion during some time interval in the discharge, as seen in Fig. 3, while the plasma parameters are either constant or slowly varying. Therefore, individual database entries do not all define threshold parameters, but rather provide the constraints from which threshold scalings can be derived. Along with standard least-square regression methods, a multivariate logistic regression technique[23] is employed to determine the parameters of a discriminant function between stable and unstable regimes.

1. Density scaling

Prior experiments have all concluded that the threshold perturbation required to initiate a locked mode is a nearly linear function of plasma density. Single parameter scans, in which density is varied at fixed B_T, plasma current, geometry, q_{95}, etc. were carried out to elucidate the dependence in the C-Mod parameter regime. An example of such a dataset, taken with a single A-coil configuration (both polarities), is shown in Fig. 8, which shows both locked and unlocked points as a function of the applied field. Experiments were carried out with steady A-coil current and either steady or decreasing density waveforms. Because of the finite intrinsic error the locking data are not symmetric about zero, but about a value corresponding to the (negative) projection of the intrinsic error field along the orientation of the applied field; such a plot is the one-dimensional analog of the circle plot of Fig. 4. If the intrinsic fields were perfectly canceled, we would expect the minimum locking density to lie arbitrarily close to zero; the fact that no unlocked points are obtained below about 2.5×10^{19} m^{-3} for this configuration is due to imperfect alignment of the applied and intrinsic fields, and also potentially to a mismatch between the poloidal mode spectra. Fitting to a function of the form $|\vec{B}_{21}^{app}+\vec{B}_{21}^{intr}| = Cn_e^{\alpha_n}$, where the fit is done for both components of $\vec{B}_{21}^{intr}$, the exponent α_n, and the coefficient of proportionality C, produces the dashed curve, which corresponds to $\alpha_n = 0.98\pm0.42$. The fitted value of the intrinsic error field in this case is $[(-4.5\pm0.5)+j(-5.1\pm1.3)]\times10^{-4}$ T, which is to be compared to an average (2; 1) intrinsic error-field inferred from the model of Sec. III B of $(-4.8-1.7j)\times10^{-4}$; in view of the error bars on the individual terms of the model (see Fig. 5), this may be taken as reasonable agreement.

2. Safety factor and toroidal field scaling

The *intrinsic* locked mode density threshold in C-Mod was determined as the safety factor was scanned over the range $3\leqslant q_{95}\leqslant4.7$; two scans were accomplished: varying B_T at constant I_p and varying I_p at constant B_T. For these experiments, the threshold was determined by decreasing the density in time from an initially stable value until locking was observed. The results are plotted in Fig. 9. The primary data are the locking densities n_L, which we may relate to the threshold error field by assuming the linear correlation determined in the preceding section. Alternatively, we may use

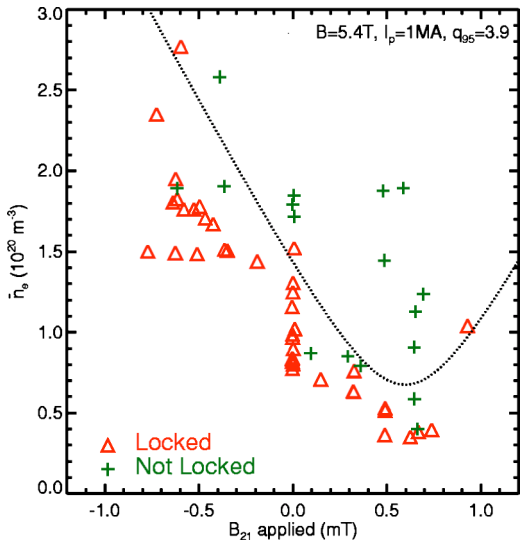

FIG. 8. (Color online). Locked (triangles) and unlocked (crosses) shots from a density scaling experiment at 1 MA, 5.4 T. The dotted curve is a discriminant function delineating locked and unlocked regions and corresponds to $\alpha_n\approx1$ and an intrinsic error of about 7×10^{-4} T.

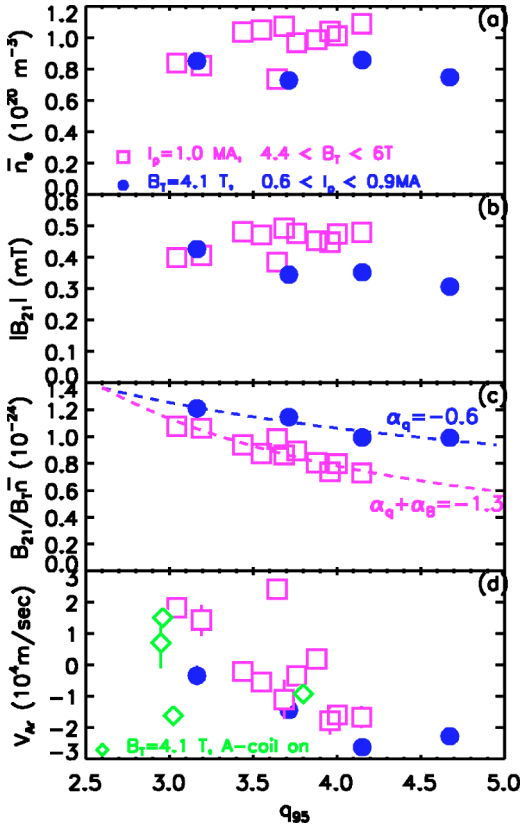

FIG. 9. (Color online). (a) Intrinsic locking density as a function of q_{95} for constant field (solid circles) and constant current (open squares). (b) Intrinsic (2,1) error field at locking as calculated from the source model of Sec. III B. (c) Fit to Eq. (4) holding α_n=1 fixed. (d) Core rotation velocity as measured by Ar Doppler system, including additional (locked and unlocked) cases with A-coil energized; velocity for locking shots evaluated before mode penetration.

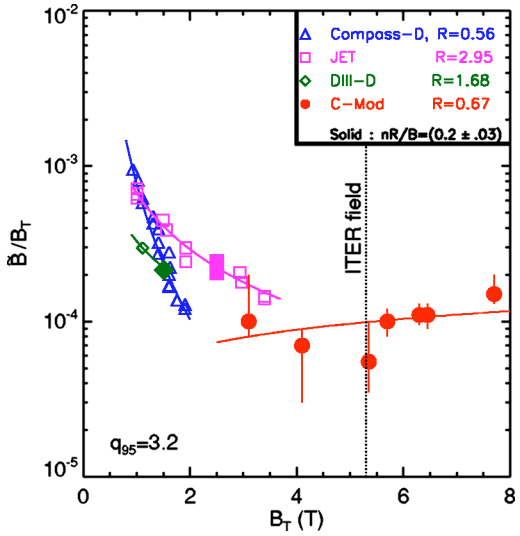

FIG. 10. (Color online). Threshold perturbation as a function of toroidal field for several tokamaks at $q_{95}=3.2\pm0.3$. The C-Mod points have $nR/B \approx 0.2\times10^{20}$ m^{-2}/T and the ordinate corresponds to B_{21}/B_T. DIII-D, Compass-D, and JET points (taken from Ref. 4) are at fixed $n=1.6\times10^{19}$ m^{-3}, and correspond to the effective perturbation B_{pen}. Points corresponding to the same nR/B as the C-Mod points are shown as solid.

the model of the intrinsic error field developed in Sec. III B directly, subject to the uncertainty of the model and especially to the lack of information regarding any possible direct contribution of asymmetries in the toroidal field coil.

We note that the current scan is essentially constant in n_L over the full range of q_{95} considered, while for the B_T scan n_L is a weakly increasing function of q_{95}. If the intrinsic error were constant this result would imply $\alpha_q \approx 0$, and $\alpha_B > -1$ where we adopt the formulation of Ref. 4,

$$\frac{B_{\rm pen}}{B_T} \propto n^{\alpha_n} B^{\alpha_B} q^{\alpha_q} R^{\alpha_R}. \tag{4}$$

In fact, the model calculation of the intrinsic error for these data actually mimics the trends seen in the density, with the magnitude $|B_{21}^{\rm intr}|$ weakly decreasing with q_{95} for the current scan and weakly increasing for the field scan. This behavior is consistent with our expectations in that the TF bus field will increase with B_T, while decreasing I_p will decrease the current in the EF3 equilibrium field coil.

Fixing $\alpha_n=1$ and fitting the data of Fig. 9(c) for the B_T and I_p scans separately gives $\alpha_q=-0.57\pm0.15$ and $\alpha_B+\alpha_q=-1.29\pm0.17$, which combine to yield $\alpha_B \approx -0.72\pm0.22$, where the quoted uncertainties are only statistical and do not include systematic errors arising from use of the intinsic field model.

The inverse correlation with q_{95} observed in these data is in contradiction to the trends reported by other experiments,[4] where either a positive or negligible correlation is reported. While the present result may be an artifact due to errors in the source model, there does seem to be a strong correlation with the observed variation of the core rotation in the same discharges, also depicted in Fig. 9.

The dependence of the threshold on toroidal field is of primary significance in extrapolating results of present experiments to the burning plasma and reactor regimes.[1] Moreover, the scaling with B_T is the point of greatest disparity among previous experiments,[4] implying that the single power law ansatz of (4) is not universally applicable. The error-field experiments on C-Mod are the first to be carried out at fields equal to and above those projected for ITER.

Figure 10 shows data from the C-Mod database at fixed q_{95} and $\bar{n}R/B$ (which for constant q_{95} is approximately the same as the Greenwald parameter and provides a convenient normalization for density across devices). These data are compared with results from three other tokamaks.[4] Points at the same $\bar{n}R/B$ from JET and DIII-D are shown as solid (the Compass-D data are all at lower $\bar{n}R/B$). The significance of these data is that, when equivalent operating conditions are considered, there appears to be very little dependence of the threshold on field or size among these devices.

With reference to Eq. (4) and again assuming $\alpha_n=1$, the C-Mod data correspond to $\alpha_B=-0.6\pm0.6$, compared to values of −1.2, −0.96, and −2.9 for JET, DIII-D, and Compass-D, respectively. (Note that the curve shown in Fig. 10 represents $(\alpha_B+\alpha_n)$ since the density is proportional to B_T for the C-Mod points.) The C-Mod results appear to reflect a weaker negative scaling with field than obtained elsewhere, although within the uncertainties they may be compatible with the DIII-D and JET scalings. A systematic, controlled parameter scan should help to clarify this dependence.

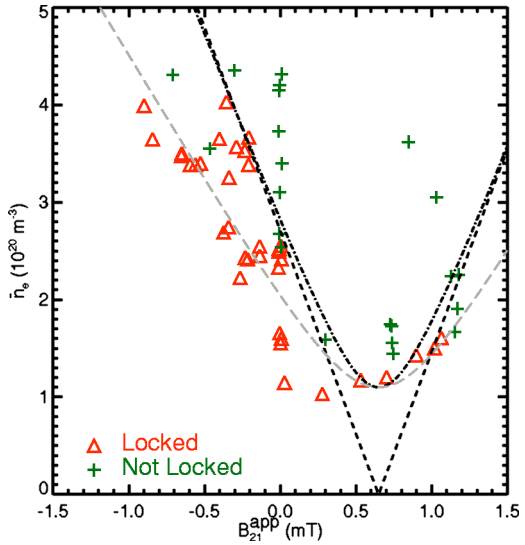

FIG. 11. (Color online). C-Mod locking region for the JET/C-Mod nondimensionally identical plasmas. Crosses denoted unlocked plasmas, triangles locked.

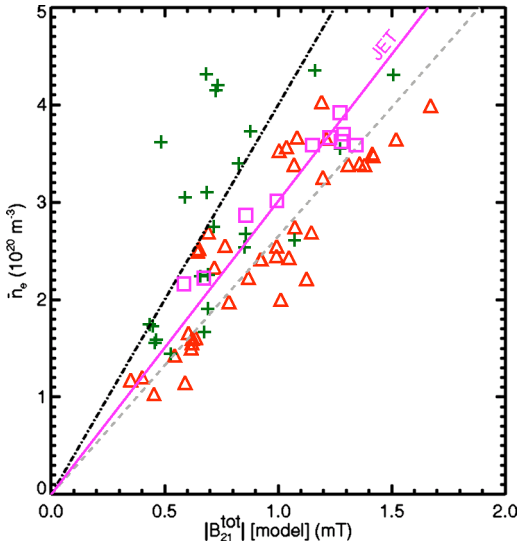

FIG. 12. (Color online). Dimensionlessly scaled JET locking threshold (squares) compared with C-Mod locked (triangles) and unlocked (crosses) data. The two dashed curves correspond to the limiting curves obtained from the raw data of Fig. 11, and the C-Mod total B_{21} points are evaluated based on the model of the intrinsic sources.

3. Nondimensional identity experiments

To better establish the scaling of the locking threshold, a specific experiment[24] has been performed to compare results from JET, C-Mod, and DIII-D in nondimensionally similar configurations.[25,26] The shapes of the plasma were matched in each machine, the safety factor fixed at $q_{95}=3.2$, while density and toroidal field were scaled as $n \propto R^{-2}$ and $B \propto R^{-5/4}$. This called for operation of C-Mod at $B_T = 6.3$ T, $I_p = 1.3$ MA. Heating was purely ohmic. Density and temperature profiles, when scaled accordingly, were observed to agree well. A wide density range (>factor of 4) was investigated. The poloidal mode spectra of the applied $n=1$ perturbations were also matched. The C-Mod coil configuration ("C" from Fig. 2) provided a good match to the (positive m) spectrum of the JET error-field correction coils. However this configuration has nominal $(m=2, n=1)$ phase −0.3 radians (fourth quadrant), which is not well aligned with the intrinsic error field (see Fig. 6).

If the locking threshold is governed completely by plasma physics, then the nondimensional threshold B_{21}/B_T should be identical in these experiments. In this case, the scaling of the error-field sensitivity with size can be inferred from the nondimensional constraint. For the power law scaling (4) we have

$$\alpha_R = 2\alpha_n + \tfrac{5}{4}\alpha_B \qquad (5)$$

allowing the requirements for ITER to be extrapolated from present experiments. While reasonable, the assumption that only plasma physics considerations determine the threshold is not guaranteed. For example, the threshold theoretically depends on the rotation profile, which may be partially determined by a boundary condition involving charge exchange momentum loss, which is governed by atomic physics and does not satisfy the condition for Connor–Taylor invariance.

In Fig. 11 we show the experimental results from the C-Mod experiment. There is some intermingling of locked and unlocked plasmas, which we attribute to hidden variability. Because of this, we show two extreme hyperbolic fits corresponding to $B_{21}^{tot}/\bar{n}_e = 2.5$ (chain curve) and 3.7(dashed) $\times 10^{-24}$ T m^3. Both fitted intrinsic error $(m=2)$ phases are close to −3 radians. The presence of the intrinsic error compromises the error-field spectrum match to some extent, since the intrinsic sideband spectrum is uncontrolled.

Using the C-Mod model of intrinsic field discussed in the preceding section, we can perform a broader comparison, including additional data from two other A-coil configurations with phase angles of −0.7 and 1.9 radians, respectively, and converting to total B_{21} amplitude using the modeled rather than fitted intrinsic field. Figure 12 shows the result: the agreement between C-Mod and the scaled JET results is clearly well within the experimental uncertainty, consistent with dimensionless identity. Initial analysis of the DIII-D data suggests that the threshold B_{21} is higher than that of C-Mod and JET for a given (scaled) density. Possible reasons for this discrepancy are being investigated.

To the extent that the nondimensional identity of the thresholds is confirmed, the predictive extrapolation to future devices, e.g., ITER, is accomplished by inferring a size scaling from the dimensionality constraint (5). Taking the consensus value $\alpha_n = 1$, the range of values for α_R obtained from $-1.2 < \alpha_B < -0.6$ is $0.5 < \alpha_R < 1.25$, suggesting a weak to moderate favorable scaling with size. A dedicated field scaling experiment on C-Mod, using the same shaping, q_{95}, and A-coil configuration should further refine this estimate.

C. Error-field correction—increased operational space

A major motivation for installing the C-Mod A-coil system was to increase the accessible operating space, particularly in the direction of higher current (increased confinement, β limits) and lower density (reduced collisionality). The degree to which this goal can be accomplished with a

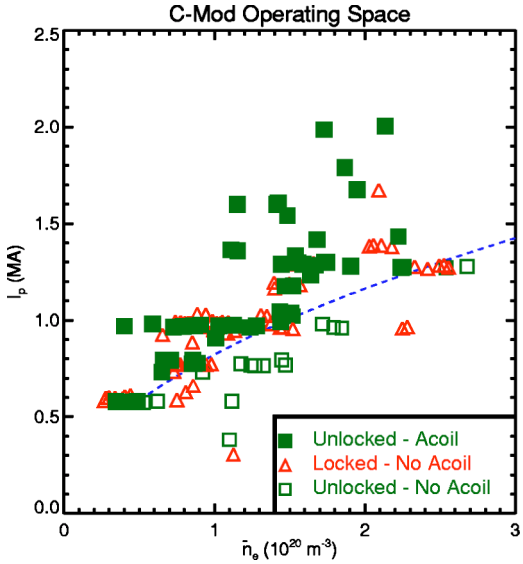

FIG. 13. (Color online). Range of locked mode free operation in C-Mod. The dashed line approximates the locking boundary without use of the A-coils (open squares are unlocked, open triangles locked); solid squares show the increased range accessible by using the A-coils to compensate the intrinsic error fields.

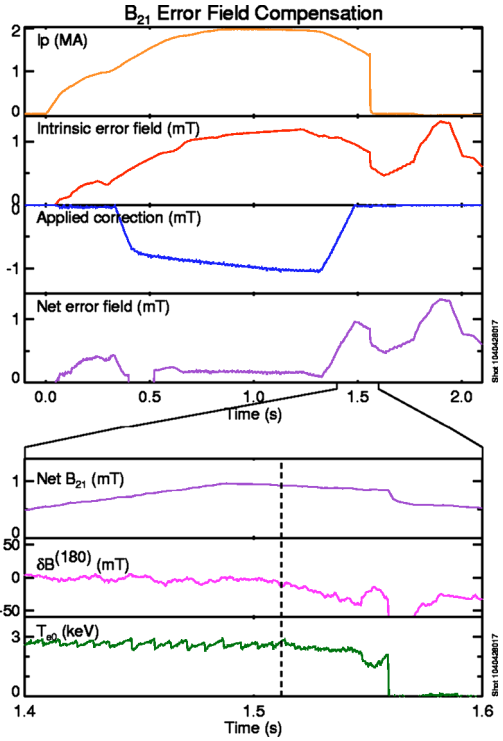

FIG. 14. (Color online). The A-coil is used to compensate the (2,1) intrinsic field error in a 2 MA discharge. Time histories of the calculated intrinsic, applied, and total B_{21} fields indicate good cancellation of the ~1 mT intrinsic error. Shortly after the A-coil is ramped down at 1.5 a locked mode appears, shortly followed by a disruption.

simple external system, remote from the plasma, may bear on the design of correction coils for future devices.

Figure 13 shows the low-density portion of the C-Mod operational regime in $(\bar{n}, I_p)$ space. Without compensation of the intrinsic field errors, operation above the dashed line almost always results in the appearance of locked modes. The improvement resulting from the use of the A-coil, about a factor of 2 in current at a given density, is shown by the solid squares. The maximum current has been increased to 2 MA, and the minimum stable density at 1 MA decreased, by about a factor of 4, to $<3\times10^{19}$ m^{-3}.

An example of a 2 MA, 8 T discharge is shown in Fig. 14. The intrinsic (2,1) error is calculated to be over 1 mT, which is compensated by use of the A-coil in the standard suppression configuration (Config. *A* in Fig. 2). Shortly after the end of current flattop, the A-coil is ramped down, and the net error field again rises to about 1 mT, leading to onset of a locked mode at $t=1.51$ s, followed by a terminating disruption shortly thereafter.

It is noteworthy that these improvements are obtained despite the fact that, owing to the orientation of the intrinsic modes, only the (2,1) component of the intrinsic error is being compensated, and in fact the magnitude of the (1,1) sideband is increased by application of the A-coil; the calculated value of $B_{11}\approx4$ mT and $B_{31}\approx0.9$ mT in the flattop of the 2 MA shot depicted in Fig. 14. This result implies that on C-Mod the sideband terms are small and cancellation of the principal (2,1) component is sufficient for stability.

V. SUMMARY

Experiments on Alcator C-Mod have extended error-field-induced locked mode studies to $B_T\sim8$ T, into the range of proposed burning plasma experiments and reactors. Intrinsic nonaxisymmetric error fields or applied perturbations with magnitude of the (2,1) helical fourier component of the order of $10^{-4}B_T$ are found to destabilize stationary islands. This threshold is similar to that found on larger, lower field devices such as JET and DIII-D in comparable operational regimes, and suggests that sensitivity to error fields is not a strong function of machine size.

Locked mode behavior on C-Mod exhibits many of the same phenomenologies as observed on other tokamaks, including modification of sawtooth behavior, braking of core rotation, and decrease in particle and energy confinement. Scaling of threshold with density is found to be essentially linear, as observed in other experiments. However, the dependence of the threshold on toroidal field and safety factor, while subject to significant uncertainties, seems to diverge from prior results. In particular, the dependence on field, expressed in terms of α_B, is less negative than on JET and DIII-D, and far less negative than Compass-C or Compass-D. The scaling with safety factor appears to be weakly negative, in contrast to prior experiments, and may be correlated with the behavior of the core rotation in C-Mod ohmic plasmas. Despite these caveats, dimensionlessly matched discharges in JET and C-Mod seem to confirm Connor–Taylor scale invariance of the locked mode thresholds, providing support for extrapolation to future devices on that basis; the resulting projections to ITER indicate that the error-field amelioration required is within the design capability of the proposed correction coil system.

Analysis of nonaxisymmetric field errors produced by the PF system on the basis of *in situ* measurements using

standard equilibrium magnetics diagnostics has resulted in a model for the error-field sources that is quantitatively consistent with the results of locked mode suppression and generation experiments, at the level of $B_{21}/B_T \sim 1\text{–}2 \times 10^{-4}$.

The successful application of the A-coil system to compensation of the intrinsic error field has resulted in substantial increases in the accessible operating space on C-Mod, including operation at up to 2 MA and Greenwald parameter $n/(I/\pi a^2)$ down to 0.04. The fact that these results are obtained with an applied mode spectrum which can effectively compensate only the (2,1) component of the intrinsic error field implies that detailed tailoring of the mode spectrum may not be required in order to suppress locked modes.

ACKNOWLEDGMENTS

Alcator C-Mod and the MIT authors are supported by U.S. Department of Energy Cooperative Agreement No. DE-FC02–99ER545512. UK authors are supported by Euratom and UK Engineering and Physical Sciences Research Council. General Atomics authors are supported by U.S. Department of Energy under Grant No. DE-FC02-04ER54698 and those from U. Texas by U.S. Department of Energy Grant No. DE-FG03-96ER5473.

[1] I. P. B. Editors, Nucl. Fusion **39**, 2286 (1999).
[2] I. H. Hutchinson, R. Boivin, F. Bombarda, P. Bonoli, S. Fairfax, C. Fiore, J. Goetz, S. Golovato, R. Granetz, M. Greenwald *et al.*, Phys. Plasmas **1**, 1511 (1994).
[3] T. C. Hender, R. Fitzpatrick, A. W. Morris, P. G. Carolan, R. D. Durst, T. Edlington, J. Ferreira, S. J. Fielding, P. S. Haynes, J. Hugill *et al.*, Nucl. Fusion **32**, 2091 (1992).
[4] R. J. Buttery, M. De'Benedetti, D. A. Gates, Y. Gribov, T. C. Hender, R. J. La Haye, P. Leahy, J. A. Leuer, A. W. Morris, A. Santagiustina *et al.*, Nucl. Fusion **39**, 1827 (1999).
[5] R. J. La Haye, R. Fitzpatrick, T. C. Hender, A. W. Morris, J. T. Scoville, and T. N. Todd, Phys. Fluids B **4**, 2098 (1992).
[6] J. T. Scoville and R. J. La Haye, Bull. Am. Phys. Soc. **40**(11), 1788 (1995).
[7] J. T. Scoville and R. J. La Haye, Nucl. Fusion **43**, 250 (2003).
[8] G. M. Fishpool and P. S. Haynes, Nucl. Fusion **34**, 109 (1994).
[9] R. J. Buttery, M. De' Benedetti, T. C. Hender, and B. J. D. Tubbing, Nucl. Fusion **40**, 807 (2000).
[10] R. Fitzpatrick and T. C. Hender, Phys. Fluids B **3**, 644 (1991).
[11] T. H. Jensen, A. W. Leonard, R. J. La Haye, and M. S. Chu, Phys. Fluids B **3**, 1650 (1991).
[12] R. J. La Haye, A. W. Hyatt, and J. T. Scoville, Nucl. Fusion **32**, 2119 (1992).
[13] R. Fitzpatrick, Nucl. Fusion **33**, 1049 (1993).
[14] R. Fitzpatrick and T. C. Hender, Phys. Plasmas **1**, 3337 (1994).
[15] R. Fitzpatrick, Phys. Plasmas **1**, 3308 (1994).
[16] E. Lazarro, R. J. Buttery, T. C. Hender, P. Zanca, R. Fitzpatrick, M. Bigi, T. Bolzonella, R. Coelho, M. DeBenedetti, S. Nowak *et al.*, Phys. Plasmas **9**, 3906 (2002).
[17] M. S. Chu, R. J. La Haye, M. E. Austin, L. L. Lao, E. A. Lazarus, A. Pletzer, C. Ren, E. J. Strait, T. S. Taylor, and F. L. Waelbroeck, Phys. Plasmas **9**, 4584 (2002).
[18] R. J. La Haye, General Atomics, San Diego, CA, Report No. GA-A22468, 1997.
[19] R. Vieira, J. Rosati, E. Fitzgerald, W. Beck, S. Wolfe, I. Hutchinson, J. Irby, W. Cochran, and D. Terry, *IEEE, Proceedings of the 20th IEEE/NPSS Symposium on Fusion Engineering (SOFE)*, edited by C. Wong (IEEE, San Diego, CA, 2003), p. 569.
[20] *Standard Handbook for Electrical Engineers*, 11th ed., edited by D. G. Fink and H. W. Beaty (McGraw-Hill, New York, 1978), pp. 4–18.
[21] R. J. La Haye and J. T. Scoville, Rev. Sci. Instrum. **62**, 2146 (1991).
[22] P. C. Hansen, *Rank-Deficient and Discrete Ill-posed Problems*, Monographs on Mathematical Modeling and Computation (Society for Industrial and Applied Mathematics, Philadelphia, 1998).
[23] D. Hosmer and S. Lemeshow, *Applied Logistic Regression*, 2nd ed. (Wiley, New York, 2000).
[24] D. F. Howell, T. C. Hender, G. Cunningham, R. J. La Haye, J. T. Scoville, I. H. Hutchinson, and S. M. Wolfe, and JET EFDA Contributors, Bull. Am. Phys. Soc. **49**(8), 76 (2004).
[25] B. B. Kadomtsev, Sov. J. Plasma Phys. **1**, 295 (1975).
[26] J. W. Connor and J. B. Taylor, Nucl. Fusion **17**, 1047 (1977).